

2019

The Elusive Nitro-Functionalised Member of the IRMOF-9 Family

Luke Conte

University of Wollongong, lc779@uowmail.edu.au

Tian-You Zhou

Massey University

Omid Qazvini

Massey University

Lujia Liu

Northwestern University, Massey University

David R. Turner

Monash University

See next page for additional authors

Publication Details

Conte, L., Zhou, T., Qazvini, O. T., Liu, L., Turner, D. R., Telfer, S. G. & Richardson, C. (2019). The Elusive Nitro-Functionalised Member of the IRMOF-9 Family. *Australian Journal of Chemistry: an international journal for chemical science*, Online First A-F.

The Elusive Nitro-Functionalised Member of the IRMOF-9 Family

Abstract

The solvothermal reaction of 2-nitro-[1,1'-biphenyl]4,4'-dicarboxylic acid (H₂bpdcNO₂) with Zn(NO₃)₂·6H₂O in DMF solvent does not give a functionalised variant of IRMOF-9. Single-crystal X-ray diffraction analysis shows the major initial product of this reaction, WUF-21 (WUF = Wollongong University Framework), is a porous interpenetrated diamondoid metal-organic framework (MOF) with a secondary building unit that 'doubly straps' eight bridging bpdcNO₂ ligands in a distorted tetrahedral shape around an unusual pentazinc core. A second porous MOF phase (WUF-23) containing a large and novel dodecazinc secondary building unit forms in the same reaction and eventually predominates in solutions containing formate anion, which arises from the hydrolysis of DMF. Doping the starting ligand with [1,1'-biphenyl]4,4'-dicarboxylic acid (H₂bpdc) provides a facile way to grow nitro-functionalised IRMOF-9, hereafter denoted as WUF-22, where the dopant is carried through into the product. Activated WUF-22 is a microporous solid with an apparent Brunauer-Emmett-Teller (BET) surface area of 2497 m² g⁻¹, which matches well with geometric surface area calculations. The CO₂ adsorption properties of WUF-22 are reported.

Publication Details

Conte, L., Zhou, T., Qazvini, O. T., Liu, L., Turner, D. R., Telfer, S. G. & Richardson, C. (2019). The Elusive Nitro-Functionalised Member of the IRMOF-9 Family. *Australian Journal of Chemistry: an international journal for chemical science*, Online First A-F.

Authors

Luke Conte, Tian-You Zhou, Omid Qazvini, Lujia Liu, David R. Turner, Shane Telfer, and Christopher Richardson

1 The elusive nitro-functionalised member of the IRMOF-9 family

2 Luke Conte^A, Tian-You Zhou^B, Omid T. Qazvini^B, Lujia Liu^C, David R. Turner^D, Shane G.
3 Telfer^B and Christopher Richardson^{A, E}

4 ^A School of Chemistry and Biomolecular Science, Faculty of Science, Medicine and Health,
5 University of Wollongong, Wollongong, NSW 2522, Australia

6 ^B MacDiarmid Institute of Advanced Materials and Nanotechnology, Institute of
7 Fundamental Sciences, Massey University, Palmerston North 4442, New Zealand

8 ^C Department of Chemistry, Northwestern University, 2145 Sheridan Road, Evanston, Illinois
9 60208-3113, United States

10 ^D School of Chemistry, Monash University, Clayton, VIC 3800, Australia

11 ^E Corresponding author. Email: chris_richardson@uow.edu.au

12 **Abstract**

13 The solvothermal reaction of 2-nitro-[1,1'-biphenyl]-4,4'-dicarboxylic acid (H₂bpdcNO₂) with
14 Zn(NO₃)₂·6H₂O in DMF solvent does not give a functionalised variant of IRMOF-9. Single
15 crystal X-ray diffraction (SCXRD) analysis shows the major initial product of this reaction,
16 WUF-21 (WUF=Wollongong University Framework), is a porous interpenetrated
17 diamondoid metal-organic framework (MOF) with a secondary building unit (SBU) that
18 'doubly-straps' eight bridging bpdcNO₂ ligands in a distorted tetrahedral shape around an
19 unusual pentazinc core. A second porous MOF phase (WUF-23) containing a large and novel
20 dodecazinc SBU forms in the same reaction and eventually predominates in solutions
21 containing formate anion, which arises from the hydrolysis of DMF. Doping the starting
22 ligand with [1,1'-biphenyl]-4,4'-dicarboxylic acid (H₂bpdc) provides a facile way to grow
23 nitro-functionalised IRMOF-9, hereafter denoted as WUF-22, where the dopant is carried
24 through into the product. Activated WUF-22 is a microporous solid with an apparent surface
25 area of 2497 m²/g (BET), which matches well with geometric surface area calculations. The
26 CO₂ adsorption properties of WUF-22 are reported.

27 **Introduction**

28 We have long been interested in the functionalisation and post-synthetic modification of
29 MOFs. Within this context, we have paid special attention to the interpenetrated **pcu** lattices
30 that form from functionalised derivatives of linearly divergent [1,1'-biphenyl]-4,4'-
31 dicarboxylic acids and tetrazinc clusters.^{[1] [2]}The parent compound of this series was first

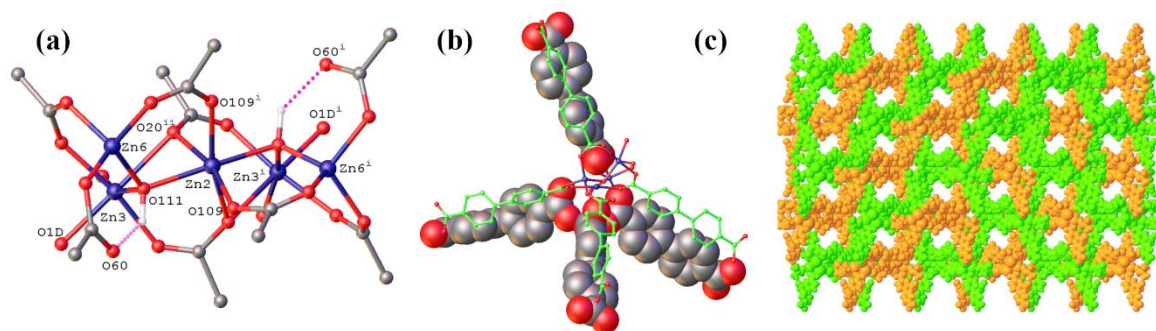
32 described by Yaghi and co-workers as part of their demonstration of isorecticular framework
33 expansion and was named IRMOF-9.^[3] It is a true testament of the power of the isorecticular
34 approach that over thirty functionalised IRMOF-9-type compounds have been described.^[2c, 4]

35 In the course of our studies we had cause to prepare the nitro-functionalised IRMOF-9
36 starting from H₂bpdcNO₂. Surprisingly, despite the popularity of H₂bpdcNO₂ as a linear
37 bridging ligand for MOFs,^[5] this IRMOF is unreported. We describe here our results of
38 preparing this complex and show that doping provides a facile way of triggering crystal
39 formation where standard methods fail.

40 **Results and Discussion**

41 Our standard solvothermal method of heating functionalised [1,1'-biphenyl]-4,4'-dicarboxylic
42 acids with a three-fold excess of zinc nitrate hexahydrate at 100 °C in DMF solvent overnight
43 has been successful for preparing many IRMOF-9 complexes.^[1a, 1b, 1d-g] However, application
44 of this methodology to the reaction with H₂bpdcNO₂ failed to yield any crystals. Varying the
45 reaction time and/or temperature and/or concentration of the DMF solution also did not result
46 in any crystal growth, much to our chagrin. The change in colour of the reaction solutions
47 from colourless to a bright yellow indicated to us that some change had taken place, and
48 several solutions were stored at room temperature. After a period of several months, three
49 types of crystals began to deposit from the solutions. After one year there were large yellow
50 and large orange crystals and smaller colourless crystals (Fig. S1-2). Single crystal X-ray
51 diffraction (SCXRD) on the orange crystals confirmed they were catena-(dimethylammonium
52 tris(μ₂-formato)zinc(II) (CSD code DAXNIA01).^[6] The large yellow crystals were
53 agglomerates and could be cleaved to give smaller individual crystals. SCXRD analysis on
54 these crystals and the smaller colourless rods (Fig. S2) revealed the structure crystallised in
55 the monoclinic space group *C2/c*. The asymmetric unit contains two zinc-carboxylate clusters
56 each consisting of one half Zn atom and two full Zn atoms with two bpdcNO₂ linkers
57 bridging between the clusters. Each cluster then coordinates another bpdcNO₂ linker (Fig.
58 S3). The clusters are differentiated by Zn3 in one cluster binding two DMF ligands whereas
59 Zn5 in the other cluster coordinates a DMF ligand and an aqua ligand. The remaining atom in
60 each cluster is a μ₃-hydroxido moiety and this participates in a H-bond with a non-
61 coordinated carboxylate oxygen of a bridging bpdcNO₂ linker (Fig. 1a). This gives a final
62 formulation for this MOF of [Zn₅(μ₃-OH)₂(bpdcNO₂)₄(DMF)₃(H₂O)], hereafter denoted as
63 WUF-21. By virtue of Zn1 and Zn2 lying on two-fold axes, the SBUs are pentazinc clusters
64 with the central Zn1 and Zn2 atoms in each cluster being 6-coordinate and distorted

65 octahedral in geometry. Figure 1a shows the SBU based on Zn2, Zn3 and Zn6 and the
 66 hydrogen bonding between μ_3 -hydroxido and carboxylate groups. The coordination geometry
 67 of Zn3 may be considered distorted octahedral with a very long bond to a μ_2 -bridging
 68 carboxylate oxygen (Zn3 \cdots O20ⁱⁱ, 2.364(12) Å) and Zn6 is four-coordinate with tetrahedral
 69 geometry. The pentazinc SBUs coordinate eight bridging bpdcNO₂ ligands in total, and these
 70 extend from the SBUs in pairs and in a distorted tetrahedral shape, making this a particularly
 71 bulky SBU (Fig. 1b). The combination of tetrahedral nodes and linear links reticulate into a
 72 diamondoid network (**dia**) with large pores. The pore space is partly occupied by an
 73 interpenetrating framework but there are pores in the structure parallel to the *c*-axis, as shown
 74 in Fig. 1c. The porosity in the structure is supported by a void volume calculation in
 75 PLATON,^[7] which returned a value of 49% of the unit cell.

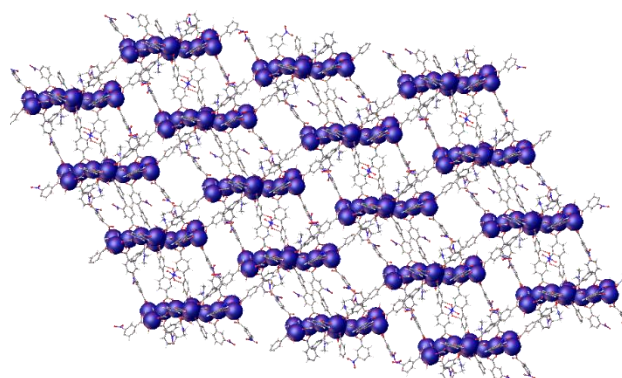


76
 77 **Fig. 1.** (a) A view of the pentazinc SBU of WUF-21, with selective atom labelling, based on
 78 Zn2, Zn3 and Zn6 showing the coordination geometries about the metal atoms and hydrogen
 79 bond to O60. Atoms superscripted with i and ii are generated through the symmetry
 80 transformations $-2-X, +Y, \frac{1}{2}-Z$ and $\frac{1}{2}+X, -\frac{1}{2}+Y, 1+Z$, respectively. (b) A view accentuating
 81 the tetrahedral shape of a SBU with foreground ligands coloured in green set ahead of ligands
 82 in space-filling form, and (c) a view parallel to the *c*-axis of the interpenetrating frameworks,
 83 displayed in green and gold, of WUF-21. Hydrogen atoms have been omitted for clarity in 1b
 84 and 1c.

85 Another morphology of crystal generally prevailed with time. Synchrotron diffraction
 86 data revealed the complex crystallises in the space group P-1 with an asymmetric unit
 87 containing twelve Zn centres, sixteen half-ligands of which nine bear nitro groups, four
 88 bridging formates, four μ_3 -hydroxido linkages, six aqua ligands, two bound DMF and a
 89 further two DMF solvate molecules, giving a formula of $[\text{Zn}_{12}(\text{bpdcNO}_2)_8(\mu_4\text{-O}_2\text{CH})_4(\mu_3\text{-}$
 90 $\text{OH})_4(\text{DMF})_2(\text{H}_2\text{O})_6 \cdot 2\text{DMF}]$ and was named WUF-23. The half-ligands connect so that intact

91 bpdcNO₂ bridging ligands are formed with full occupancy nitro groups. The zinc centres are
92 assembled into a dodecazinc platter by bridging carboxylate and formate connectors. By
93 virtue of the sixteen half-ligands that project from the platter, not only does this SBU have
94 high nuclearity but also high connectivity (Fig. S4). Eight octahedrally-coordinated zinc
95 centres run along a central vein with the remaining four tetrahedrally-coordinated centres
96 around the platter's periphery. The μ_3 -hydroxido moieties and the monodentate aqua ligands
97 attached to Zn6 and Zn7 show stabilising intra-SBU H-bond interactions with carboxyl
98 groups. Other zinc centres coordinate monodentate ligands: Zn1 and Zn12, which can be
99 considered the terminal metal centres, each coordinate two aqua ligands, and Zn4 and Zn9
100 coordinate the DMF ligands.

101 The expanded structure is highly porous and a PLATON calculation returned a
102 solvent accessible volume of 58% of the unit cell. Alongside the high porosity is a tortuous
103 pore system. Channels are evident parallel to each of the crystallographic axes (100, $\sim 10 \times 12$
104 \AA ; 010, $\sim 12 \times 14 \text{\AA}$; 001, $\sim 12 \times 18 \text{\AA}$) as well as the 110 and 111 directions (Fig. S5-S8). A
105 view of the channel system permeating along the crystallographic 100 direction is shown in
106 Figure 2. The formation of this phase is dependent on sufficient formate being available as it
107 plays a crucial role in the assembly of the SBU. The appearance of this phase and catena-
108 (dimethylammonium tris(μ_2 -formato)zinc(II) is consistent with the hydrolysis of DMF during
109 solvothermal treatment and in the ageing solutions.

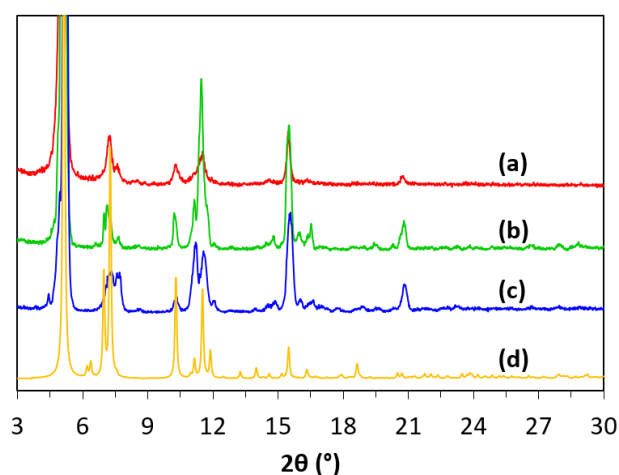


110

111 **Fig. 2.** (a) A view parallel to the crystallographic *a*-axis with zinc atoms shown in space-
112 filling form to identify the positions of the dodecazinc SBUs in WUF-23.

113 With our curiosity piqued by nitro-functionalised IRMOF-9 crystals failing to grow
114 under our standard conditions, we hypothesised that doping H₂bpdcNO₂ with H₂bpdc, the
115 latter of which forms the IRMOF-9 structure, would solve this problem. Our hypothesis being
116 that H₂bpdc would trigger crystal formation allowing for the nitrated ligand to be

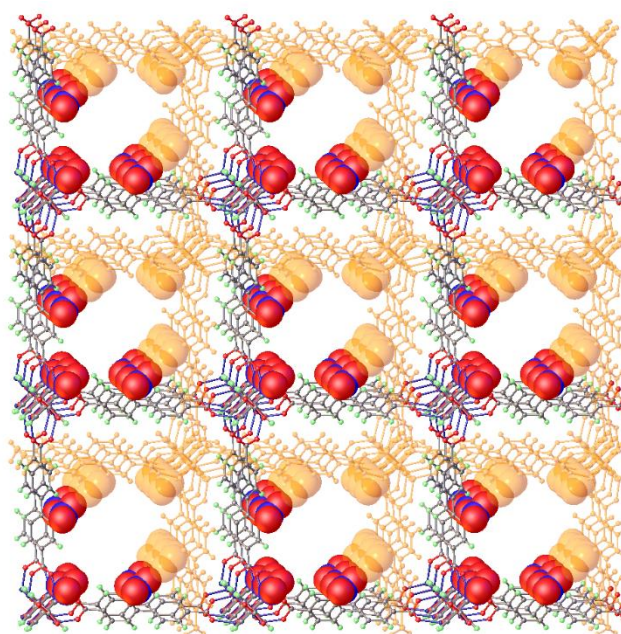
117 incorporated in the growing lattice. In order to find the minimum amount of dopant needed,
118 we spiked H₂bpdcNO₂ with small proportions of H₂bpdc (4mol%, 6mol%, 9mol% and
119 12mol% of H₂bpdc, as estimated by integration of ¹H NMR spectra (Fig. S12-16), and
120 reacted each mixture with three equivalents of zinc nitrate in DMF under identical conditions
121 of solution concentration, time and temperature. No crystal formation was observed with the
122 reaction containing 4mol% doping and the WUF-21 structure formed after many months.
123 Each of the other reactions gave clumps of crystals during heating overnight and the PXRD
124 patterns of these samples showed good correlation to IRMOF-9 (Fig. 3; Fig. S21-23). This
125 result clearly indicates a lower threshold exists for effective doping to direct phase selection
126 in this system.



127
128 **Fig. 3.** PXRD patterns of the MOF samples from the doping experiments at (a) 6mol% (b)
129 9mol% and (c) 12mol% of H₂bpdc and (d) the calculated pattern of IRMOF-9.
130 SCXRD analysis confirmed the crystals are nitro-functionalised analogues of IRMOF-9 and
131 were named WUF-22. The MOF crystallises as a pair of interpenetrating **pcu** networks in the
132 space group *C2/m*. This is a space group we have found to be common for functionalised
133 IRMOF-9 complexes.^[1a, 1b, 1d, 1f-h] The asymmetric unit features one full Zn atom (Zn2), two
134 half Zn atoms (Zn1, Zn3) and a half oxido atom (O1) at the centre of the SBU, in addition to
135 a quarter of a solvent water molecule occupying a special position (0.0, 0.5, 1). Zn3
136 coordinates a partially occupied water molecule (0.33). All atoms of one bpdcNO₂ linker are
137 contained in the asymmetric unit (O20 to O37), while the second ligand based on O2 to O16
138 has atoms C4, C5, C8, C11, C14 and C15 laying across a mirror plane (Fig. S9). The phenyl
139 ring carbons C6, C7, C9, C10 and the nitro group attached to this ring (N90-O92) were
140 assigned half occupancy to match the crystallographically defined disorder. Nitrogen atoms

141 of the tag groups were found in difference maps and therefore define the positions of the nitro
142 groups. These were completed in the crystallographic model by attaching oxygen atoms in
143 fixed representative positions in the structure. Further details concerning the refinement can
144 be found in the Supplementary Information.

145 The close association of the frameworks is sustained by short contacts (~ 2.6 Å)
146 between C-H bonds of one framework to a carboxylate oxygen in the SBU of the partner
147 framework [H7 \cdots O36, ($\frac{1}{2}$ -X, $\frac{1}{2}$ +Y, 1-Z)]. This results in the largest pores in this structure
148 running parallel to the crystallographic *c*-axis, which are lined with nitro groups (Fig. 4). The
149 shortest atom-centre-to-atom-centre distances (*i.e.* excluding Van der Waals contact
150 distances) in these pores range from 6-9 Å between nitro groups (Fig. S10) with distances
151 around 10.5 Å for most other interatom contacts around the pore environment.



152
153 **Fig. 4.** A view slightly offset from the crystallographic *c*-axis of WUF-22 with the
154 interpenetrating framework shown in orange and nitro groups of both frameworks displayed
155 in space-filling form to accentuate their positioning along the pore wall.

156 We determined the proportion of bpdc linkers in the resultant phases of WUF-22 by
157 ^1H NMR spectroscopy after digesting crystals in DCI/DMSO-*d*₆ (Fig. S17-20). The results
158 showed bpdc is present in higher amounts in the crystals than was supplied by the synthesis
159 mixture at each doping level, pointing to a preferential incorporation of bpdc over bpdcNO₂
160 (Table 1). The MOFs are named WUF-22(X) where X represents the percentage
161 incorporation of bpdc. We have observed preferential incorporation of one ligand over

162 another in multivariate IRMOF-1 compounds related to crystal growth rates^[8] and in other
163 IRMOF-9 compounds related to steric reasons.^[1g] We postulate here that bpdc ligands
164 nucleate crystal growth and continue to be incorporated in to the structure, leading to their
165 higher proportion.

166 Yields were recorded on samples after solvent exchange with CH₂Cl₂ and vacuum
167 drying and found to depend strongly on the doping level (Table 1). The yield of 34%
168 obtained at the highest doping level of 12mol% of H₂bpdc in H₂bpdcNO₂ is comparable with
169 yields we have obtained in non-doped IRMOF-9 systems. As this doping level gave the
170 highest yield, WUF-22(14) was used for all further analyses. In addition, in subsequent
171 preparations, clumps of crystals formed by ~16 h were split apart with a spatula and this
172 resulted in the growth of many small cubic-shaped crystals of WUF-22(14) over the next few
173 hours.

174 Table 1. Yields and formulations of the IRMOFs formed from different doping levels.

Mol% of H ₂ bpdc in H ₂ bpdcNO ₂	Yield (%)	Mol% of bpdc in MOF	MOF Formulation	Name
6	9	8	Zn ₄ O(bpdc-NO ₂) _{2.77} (bpdc) _{0.23}	WUF-22(8)
9	18	10	Zn ₄ O(bpdc-NO ₂) _{2.71} (bpdc) _{0.29}	WUF-22(10)
12	34	14	Zn ₄ O(bpdc-NO ₂) _{2.59} (bpdc) _{0.41}	WUF-22(14)

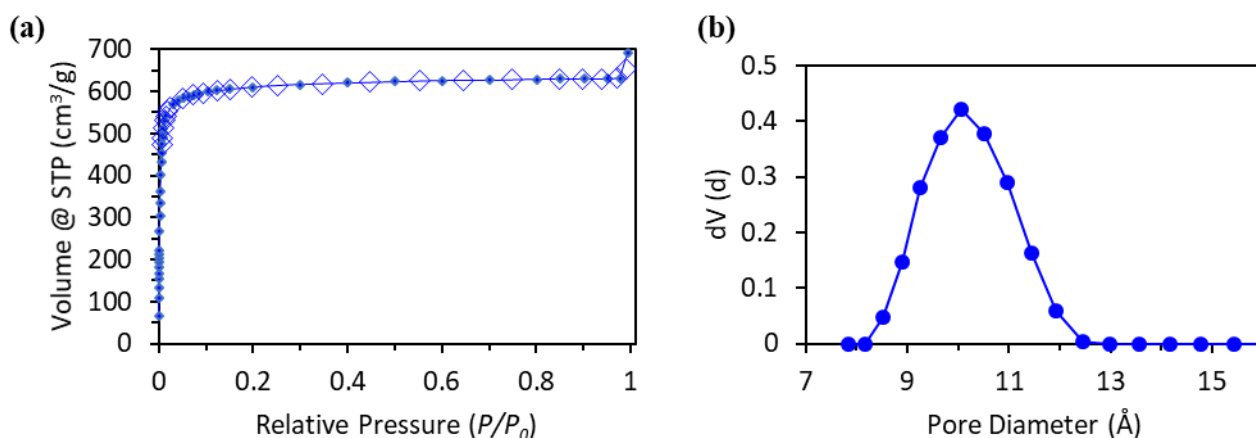
175

176 Gas Adsorption Studies

177 PXRD patterns recorded after manual separation of the visibly discernible zinc formate
178 crystals showed the remaining crystals were mixtures of WUF-21 and WUF-23, as expected
179 (Fig. S24). Furthermore, solvent exchange of the mother liquor for fresh DMF resulted in
180 visible degradation of the crystals. For these reasons, activation and gas sorption studies were
181 not pursued.

182 Crystals of WUF-22(14) were used to study surface area and gas adsorption properties
183 after solvent exchange with acetone then cyclohexane and activation by freeze-drying and
184 heating under dynamic vacuum at 120 °C. Simultaneous thermogravimetric analysis-
185 differential scanning calorimetry (TG-DSC) on activated WUF-22(14) showed no thermal

186 events in the sample until framework decomposition (Fig. S25). This contrasts with our work
 187 on a strontium-based MOF of this ligand (WUF-15) where exothermic loss of the nitro group
 188 was observed.^[9] The N₂ isotherm at 77 K is Type I (Fig. 5) and consistent with the expected
 189 microporosity of IRMOF-9-type compounds. The apparent BET surface area calculated in the
 190 range 0.008-0.04 P/P_0 was 2497 m²/g with a pore volume of 0.901 cm³/g at 0.95 P/P_0 . Pore
 191 size analysis derived from DFT calculations determined a tight distribution clustered around
 192 10 Å (Fig. 5b) and this agrees well with the results from SCXRD.



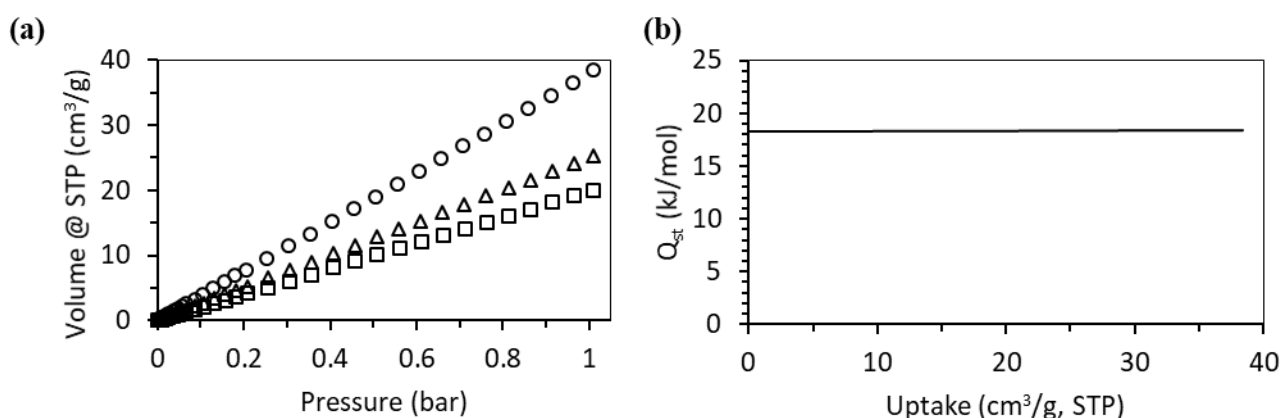
193
 194 **Fig. 5.** (a) The N₂ isotherm at 77 K with adsorption points as filled diamonds and desorption
 195 points as open diamonds, and (b) the pore size distribution from DFT analysis of WUF-
 196 22(14).

197 To support our experimental results, we performed surface area calculations using the
 198 method of Snurr with a probe atom radius set to 3.72 Å to match dinitrogen.^[10] Ordered
 199 models containing four tetrazinc clusters and twelve unique ligands in the unit cell were
 200 constructed with formula's [(Zn₄O)₄(bpdc-NO₂)₁₁(bpdc)₁] and [(Zn₄O)₄(bpdc-NO₂)₁₀(bpdc)₂]
 201 to bound the formula of WUF-22(14) [(Zn₄O)₄(bpdc-NO₂)_{10.44}(bpdc)_{1.64}]. The experimental
 202 result of 2497 m²/g falls between the calculated values for [(Zn₄O)₄(bpdc-NO₂)₁₁(bpdc)₁] at
 203 2466 m²/g and [(Zn₄O)₄(bpdc-NO₂)₁₀(bpdc)₂] at 2510 m²/g, indicating a high-quality sample
 204 of WUF-22(14) with complete activation.

205 Given the nitro-functionalisation of WUF-22(14) were in interested to see how it
 206 performed in the adsorption of CO₂ and how this compared to other MOF materials.^[4f, 11] Fig.
 207 6a shows the adsorption legs of CO₂ isotherms collected at 273, 288 and 298 K up to 1 bar
 208 with full adsorption-desorption isotherms provided in Fig. S27. Each adsorption isotherm is
 209 linear and WUF-22(14) takes up a maximum of 38.5 cm³/g at 1 bar and 273 K. In comparison

210 with other functionalised IRMOF-9-type compounds from our laboratories, this value is
211 surprisingly low. As examples, sulfone-functionalised IRMOF-9 frameworks had uptakes
212 between 44 and 51 cm³/g and the uptakes of dimethylthiocarbamate-functionalised IRMOF-9
213 complexes were 49-56 cm³/g at 273 K. The poor adsorption of CO₂ is responsible for a low
214 selectivity factor over N₂ of 6.7, as determined from single-component gas isotherms at 298
215 K and a hypothetical gas composition of 16% CO₂ and 77% N₂ and 7% from other gases (see
216 SI).

217 The Q_{st} for CO₂ binding to WUF-22(14) was calculated from the adsorption
218 isotherms collected at all three temperatures after fitting them with a virial equation (Fig.
219 S28). This results in a Q_{st} of ~-18 kJ/mol across all uptake values (Fig. 6b). This modest
220 value suggests that CO₂ does not interact strongly with potential adsorption sites like the
221 frameworks nitro groups. By way of comparison, the Q_{st} for IRMOF-9 was calculated by a
222 virial method to be ~-23 kJ/mol^[4f] and the value for nitro-functionalised IRMOF-8 is ~-35
223 kJ/mol.^[11a] We note that care needs to be taken in comparisons with other MOFs, particularly
224 where the apparent BET surface areas fall well short of calculated surface areas and that to
225 determine a true measure of the interaction of CO₂ with organic functional groups in MOFs
226 requires experimental surface areas close to that from simulation or calculation. For example,
227 it is known that small amounts of remaining solvents in MOFs, particularly water, greatly
228 impacts the uptake and binding strength of the MOF toward CO₂.



229
230 **Fig. 6.** (a) Adsorption legs of the CO₂ isotherms of WUF-22(14) at 273 K (circles), 288 K
231 (triangles) and 298 K (squares), and (b) a plot of the Q_{st} profile for WUF-22(14).

232 Conclusion

233 Two novel nitro-functionalised MOFs are the products after solvothermal reaction of pure
234 H₂bpdCNO₂ with Zn(NO₃)₂·6H₂O in DMF. We have shown that spiking ligands with
235 proportions as low as 6% can effectively direct the course of MOF formation towards desired
236 products. The method is simple and capable of producing MOF materials that cannot be made
237 under normal circumstances. Here, this enabled the preparation of a nitro-functionalised
238 IRMOF-9 complex, which showed a surprisingly low affinity for CO₂ after complete
239 activation. We note the difficulty in making comparisons to other MOFs as experimental
240 surface areas need to follow closely to calculated values to ensure activation is achieved
241 without some level of structural collapse or from frameworks with high level of defects.

242 **Experimental**

243 All chemicals used were of analytical grade and purchased from Sigma Aldrich, VWR
244 Australia, or Ajax Finechem Pty Ltd. H₂bpdCNO₂ was prepared as described.^[2b] ¹H NMR
245 spectra were obtained using a Bruker Ascend 400 MHz spectrometer and referenced to the
246 residual protio peak at δ 2.50 ppm in DMSO-*d*₆. ¹H NMR analysis was performed on MOF
247 samples (~10 mg) digested by adding 35% DCl in D₂O (2.5 μL) and DMSO-*d*₆ (500 μL) and
248 stirring until a solution was obtained. Simultaneous TG-DSC data were obtained using a
249 Netzsch STA 449 F1 Jupiter instrument. Measuring parameters of 10 °C/min under a mix of
250 nitrogen (10 cm³/min) and compressed air N₂/O₂ (80/20, 10 cm³/min) were used. PXRD
251 patterns were recorded on a GBC-MMA X-ray diffractometer using Cu K(α) radiation
252 (1.5418 Å) with samples mounted on 25 mm SiO₂ substrates. The experimental data was
253 collected in the 2θ angle range of 3–30° with a step size of 0.02° and a scan speed of 1°/min.
254 SCXRD data for WUF-21 and WUF-22 were recorded on a Rigaku Spider diffractometer
255 equipped with a MicroMax MM007 rotating anode generator (Cu radiation, 1.54180 Å),
256 fitted with high flux Osmic multilayer mirror optics, and a curved image-plate detector. Data
257 were collected at 292 K and were integrated and scaled and averaged with FS process.^[12]
258 XPREP was used to determine the space group and the structure was solved using
259 SHELXT^[13] for WUF-21 and SHELXS97^[14] for WUF-22 and both refined with SHELXL.^[15]
260 Data for WUF-23 were recorded on the MX2 beamline at the Australian Synchrotron with
261 wavelength 0.71073 Å at 100 K. Two datasets were merged and truncated to 1.00 Å to give
262 97% completeness. The structure was solved by direct methods and refined using SHELXL
263 under the Olex² GUI.^[16] Further details on the collections and refinements can be found in the
264 Supporting Information to this article.

265 Gas adsorption studies up to 1 bar were carried out using a Quantachrome Autosorb MP
266 instrument and high purity nitrogen (99.999%) and carbon dioxide (99.995%) gases at the
267 Wollongong Isotope Geochronology Laboratory. Surface areas were determined using
268 Brunauer–Emmett–Teller (BET) calculations. Pore size distributions were calculated using
269 the QSDFT equilibrium kernel for N₂ at 77 K on carbon with slit/cylindrical pores as
270 implemented in the Quantachrome software (v 3.0).

271 **Synthetic procedure for WUF-21 and WUF-23**

272 In a typical experiment, H₂bpdcNO₂ (105.6 mg, 0.37 mmol) and Zn(NO₃)₂·6H₂O (365 mg,
273 1.22 mmol) were dissolved in DMF (10 mL) with stirring. The colourless solution was then
274 placed in a preheated oven at temperatures from 80 °C up to 120 °C and for times between 24
275 and 48 hours. No crystals formed in these brightly yellow coloured solutions. Samples were
276 left to stand in capped vials at ambient temperature. Crystals started forming after
277 approximately six months and some solutions were stored for over three years. No yields
278 were calculated.

279 **General procedure for WUF-22(X) synthesis**

280 H₂bpdc and H₂bpdcNO₂ in the desired molar ratio (50 mg in total combined mass) and
281 Zn(NO₃)₂·6H₂O (156 mg, 0.52 mmol) were dissolved in DMF (8 mL) with stirring. The
282 solution was then placed in a preheated oven at 100 °C for 18 hours. For WUF-22(14), any
283 clumps of crystals at this time were split apart using a spatula and heating was continued for
284 another 6 hours. The DMF solution was then exchanged three times with fresh DMF (2 mL)
285 at 100 °C and then for dry acetone at 80 °C, each for 15 minutes. The crystals were left to
286 stand under fresh dry acetone until needed for analysis at which time the solvent was changed
287 to cyclohexane at room temperature and the samples were activated by freeze-drying at –53
288 °C and 0.09 mbar for 1 hour followed by heating under dynamic vacuum at 120 °C for 6
289 hours. Details on yields and formulations are provided in Table S1.

290 **Supporting Information**

291 ¹H NMR spectra for the doped ratios of H₂bpdc in H₂bpdcNO₂, digestion spectra for WUF-
292 22(8-14), TG-DSC data for WUF-22(14), SCXRD data for WUF-21-23, PXRD patterns,
293 adsorption-desorption gas sorption isotherms for WUF-22(14), virial fitting plots and
294 parameters.

295 Crystallographic data have been deposited with the Cambridge Crystallographic Data Centre,
296 CCDC deposition numbers 1912369, 1912370 and 1937365 for WUF-21-23, respectively.

297 Copies of the data can be obtained free of charge from
298 <http://www.ccdc.cam.ac.uk/conts/retrieving.html> or from the Cambridge Crystallographic
299 Data Centre (12 Union Road, Cambridge, CB2 1EZ, UK; Fax: +44 1223 336033; Email:
300 deposit@ccdc.cam.ac.uk).

301 **Acknowledgements**

302 L.C. acknowledges the Australian Government for an Australian Government Research
303 Training Program Award. C.R. thanks the University of Wollongong for financial support.
304 This research did not receive any specific funding.

305 **Conflicts of Interest**

306 The authors declare no conflicts of interest.

307 **References**

- 308 [1] (a) A. D. Burrows, C. Frost, M. F. Mahon, C. Richardson. *Angew Chem Int Ed.* **2008**,
309 *47*, 8482; (b) A. D. Burrows, C. G. Frost, M. F. Mahon, C. Richardson. *Chem Commun.*
310 **2009**, 4218; (c) A. D. Burrows, L. C. Fisher, D. Hodgson, M. F. Mahon, N. F. Cessford, T.
311 Dueren, et al. *CrystEngComm.* **2012**, *14*, 188; (d) A. D. Burrows, S. O. Hunter, M. F. Mahon,
312 C. Richardson. *Chem Commun.* **2013**, *49*, 990; (e) M. R. Bryant, C. Richardson.
313 *CrystEngComm.* **2015**, *17*, 8858; (f) T. A. Ablott, M. Turzer, S. G. Telfer, C. Richardson.
314 *Cryst Growth Des.* **2016**, *16*, 7067; (g) M. R. Bryant, A. D. Burrows, C. J. Kepert, P. D.
315 Southon, O. T. Qazvini, S. G. Telfer, et al. *Cryst Growth Des.* **2017**, *17*, 2016; (h) M. R.
316 Bryant, T. A. Ablott, S. G. Telfer, L. Liu, C. Richardson. *CrystEngComm.* **2019**, *21*, 60.
317 [2] (a) R. K. Deshpande, J. L. Minnaar, S. G. Telfer. *Angew Chemie Int Ed.* **2010**, *49*,
318 4598; (b) D. J. Lun, G. I. N. Waterhouse, S. G. Telfer. *J Am Chem Soc.* **2011**, *133*, 5806; (c)
319 R. K. Deshpande, G. I. Waterhouse, G. B. Jameson, S. G. Telfer. *Chem Commun.* **2012**, *48*,
320 1574; (d) A. Ferguson, L. Liu, S. J. Tapperwijn, D. Perl, F. X. Coudert, S. Van
321 Cleuvenbergen, et al. *Nat Chem.* **2016**, *8*, 250.
322 [3] M. Eddaoudi, J. Kim, N. Rosi, D. Vodak, J. Wachter, M. O'Keeffe, et al. *Science.*
323 **2002**, *295*, 469.
324 [4] (a) T.-H. Park, K. Koh, A. G. Wong-Foy, A. J. Matzger. *Cryst Growth Des.* **2011**, *11*,
325 2059; (b) J. M. Roberts, O. K. Farha, A. A. Sarjeant, J. T. Hupp, K. A. Scheidt. *Cryst Growth*
326 *Des.* **2011**, *11*, 4747; (c) D. Rankine, A. Avellaneda, M. R. Hill, C. J. Doonan, C. J. Sumbly.
327 *Chem Commun.* **2012**, *48*, 10328; (d) I. Boldog, L. Xing, A. Schulz, C. Janiak. *Comptes*
328 *Rendus Chimie.* **2012**, *15*, 866; (e) W. W. Lestari, P. Lönnecke, M. B. Sárosi, H. C. Streit, M.
329 Adlung, C. Wickleder, et al. *CrystEngComm.* **2013**, *15*, 3874; (f) R. Babarao, C. J. Coghlan,
330 D. Rankine, W. M. Bloch, G. K. Gransbury, H. Sato, et al. *Chem Commun.* **2014**, *50*, 3238;
331 (g) P. V. Dau, S. M. Cohen. *Inorg Chem.* **2015**, *54*, 3134; (h) S. Glomb, D. Woschko, G.
332 Makhloufi, C. Janiak. *ACS Appl Mater Interfaces.* **2017**, *9*, 37419.
333 [5] (a) P. V. Dau, S. M. Cohen. *CrystEngComm.* **2013**, *15*, 9304; (b) L.-R. Guo, X.-L.
334 Tang, Z.-H. Ju, K.-M. Zhang, H.-E. Jiang, W.-S. Liu. *CrystEngComm.* **2013**, *15*, 9020; (c) M.
335 A. Gotthardt, S. Grosjean, T. S. Brunner, J. Kotzel, A. M. Ganzler, S. Wolf, et al. *Dalton*
336 *Trans.* **2015**, *44*, 16802; (d) S. Halis, N. Reimer, A. Klinkebiel, U. Lüning, N. Stock.
337 *Microporous Mesoporous Mater.* **2015**, *216*, 13.

- 338 [6] P. Jain, N. S. Dalal, B. H. Toby, H. W. Kroto, A. K. Cheetham. *J Am Chem Soc.*
339 **2008**, *130*, 10450.
- 340 [7] A. L. Spek. *Acta Cryst.* **2009**, *D65*, 148.
- 341 [8] A. D. Burrows, L. C. Fisher, C. Richardson, S. P. Rigby. **2011**, *47*, 3380.
- 342 [9] A. Khansari, S. G. Telfer, C. Richardson. *Cryst Growth Des.* **2018**, *19*, 268.
- 343 [10] T. Düren, F. Millange, G. Férey, K. S. Walton, R. Q. Snurr. *J Phys Chem C.* **2007**,
344 *111*, 15350.
- 345 [11] (a) S. Orefuwa, E. Iriowen, H. Yang, B. Wakefield, A. Goudy. *Microporous*
346 *Mesoporous Mater* **2013**, *177*, 82; (b) D. C. Young, H. Yang, S. G. Telfer, P. E. Kruger.
347 *Inorg Chem.* **2017**, *56*, 12224.
- 348 [12] *FSProcess, Rigaku Corporation Tokyo, Japan* **1996**.
- 349 [13] G. M. Sheldrick. *Acta Cryst.* **2015**, *A71*, 3.
- 350 [14] G. M. Sheldrick. *Acta Cryst.* **2008**, *A64*, 112.
- 351 [15] G. M. Sheldrick. *Acta Cryst.* **2015**, *C71*, 3.
- 352 [16] O. V. Dolomanov, L. J. Bourhis, R. J. Gildea, J. A. K. Howard, H. Puschmann. *J Appl*
353 *Cryst.* **2009**, *42*, 339.
- 354